Quantum Science and Technology

RECEIVED
27 July 2020

REVISED
2 November 2020

ACCEPTED FOR PUBLICATION
17 November 2020

PUBLISHED
20 January 2021

PAPER

# Tunable transverse spin–motion coupling for quantum information processing

**Adam D West*, Randall Putnam, Wesley C Campbell and Paul Hamilton**

UCLA, Department of Physics and Astronomy, 475 Portola Plaza, Los Angeles, CA 90095, United States of America
* Author to whom any correspondence should be addressed.

**E-mail:** adam@physics.ucla.edu and west@ionq.co

**Keywords:** quantum information processing, ion trapping, entanglement

Supplementary material for this article is available online

## Abstract

Laser-controlled entanglement between atomic qubits ('spins') and collective motion in trapped ion Coulomb crystals requires conditional momentum transfer from the laser. Since the spin-dependent force is derived from a spatial gradient in the spin–light interaction, this force is typically longitudinal—parallel and proportional to the average laser *k*-vector (or two beams' *k*-vector difference), which constrains both the direction and relative magnitude of the accessible spin–motion coupling. Here, we show how momentum can also be transferred perpendicular to a single laser beam due to the gradient in its transverse profile. By controlling the transverse gradient at the position of the ion through beam shaping, the relative strength of the sidebands and carrier can be tuned to optimize the desired interaction and suppress undesired, off-resonant effects that can degrade gate fidelity. We also discuss how this effect may already be playing an unappreciated role in recent experiments.

## 1. Introduction

Quantum computers based on trapped atomic ions use entanglement between the atomic qubits and collective motion to mediate conditional quantum logic between spatially separated qubits [1]. This spin–motion entanglement is produced by applying a spatially-varying interaction with an electromagnetic field that gives a spin-dependent force. In laser-driven, ion–ion entangling gates, this force is derived from the longitudinal gradient of the electric field of a laser beam (or, for Raman processes, a pair of beams), in which case the direction of spin–motion coupling is fixed by the laser beam propagation axes [2]. This precludes direct control of ion motion perpendicular to the beam, and also fixes the relative strengths of the resonant spin-only and spin–motion couplings. In many experiments using surface electrode traps, optical access is restricted to be parallel to the surface plane [3]; this restriction makes it difficult to access motion perpendicular to the plane, both for cooling and coherent operations.

Two workarounds to access out-of-plane motion are the development of traps with tilted principal axes [4–9], or the introduction of time-dependent cross-coupling potentials [10]. These indirect techniques take advantage of the approximate separability of the secular motion into components along the principal axes of the trap to provide access to part of the motion (the secular component), but direct access to the full motional state (for instance, to diagnose excess micromotion) remains challenging [7, 11]. The method presented here has the additional benefit of only requiring a single beam to couple to motion. Alternative approaches for controlling spin–motion coupling using static and near-field gradients are being pursued by some groups [12–18], however these are constrained by the fixed electrode geometry and typically have a lower associated Rabi frequency than is possible with the technique we describe here.

Here, we show that the transverse, as opposed to longitudinal, gradient of the spin–light interaction can also be used to produce and control spin–motion entanglement, even perpendicular to the laser propagation direction. By adjusting the spatial profile and/or position of the beam, the strength of motional

© 2021 IOP Publishing Ltd

sidebands can be tuned, even to the point where the carrier transition is fully suppressed. By extinguishing the carrier during sideband operations and extinguishing the sidebands during carrier operations, this flexibility has the potential to suppress errors from off-resonant transitions [19]. As a proof of principle, we demonstrate this transverse spin–motion coupling using a single trapped ion. The stimulated Raman spectrum driven in a co-propagating beam geometry shows motional sidebands driven by the beam's transverse intensity gradient, and we show that their strength can be tuned by varying the ion temperature, in agreement with the model.

## 2. Theory

We consider a laser-driven electronic transition in a single trapped ion and show how the finite transverse extent of the beam can change the motional state perpendicular to the beam, even when the (conventional longitudinal) Lamb–Dicke factor is essentially zero. Since the technique presented here is applicable to every type of electronic transition used for quantum information processing (E2, E3, stimulated Raman, etc.), we present it without reference to the details of the internal state manipulation where possible and point out where differences may arise. We assume that the wavevector of the laser field (or wavevector difference, for stimulated Raman transitions) is aligned with $+\hat{\mathbf{z}}$, which we also assume is a principal axis of the trapping potential such that the longitudinal gradient cannot couple to motion in the $x$–$y$ plane. For simplicity, we consider motion along only the $x$ direction and neglect the other two; a full treatment that includes $y$ and $z$ can be constructed in a straightforward manner. We can write the matrix element associated with this transition as

$$\Omega_{n',n} = \Omega_0 \langle n' | f(x) | n \rangle \tag{1}$$

where $n$ ($n'$) is the initial (final) motional state along $x$ and the function $f(x)$ is the transverse spatial profile of the laser-ion coupling, $\Omega(x) \equiv \Omega_0 f(x)$. We absorb all of the electronic transition details in $\Omega_0$ and assume the atomic matrix element is proportional to $f$ [1].

While the beam profile can in principle have a variety of functional forms we will first assume it is Gaussian, with $f(x) \equiv \exp(-2x^2/w^2)$ (shortly, we also consider the case of a $\mathrm{TEM}_{10}$ mode). In the case of a stimulated Raman transition, $f(x)$ describes the product of the electric fields, $E_1 E_2^*$. Assuming a co-propagating configuration where the two frequency components have identical beam profiles, $w = w_0$, the Gaussian beam waist, defined as the $1/e^2$ intensity radius. In the case of a single photon transition (e.g. E2 or E3), $f(x)$ is the profile of the electric field and $w = \sqrt{2} w_0$.

We will treat the spatial profile of the beam(s) by Taylor expanding about the ion's equilibrium position ($x = 0$) to second order in $x$. A Gaussian spatial profile that is offset from the ion's equilibrium position by a distance $d$ (that is, $f(x - d)$, as shown in figure 1(a)) produces matrix elements of the following form (up to second order in $x_0$):

$$\Omega_{n',n} = \Omega_0 f(-d) \sqrt{\frac{n_>!}{n_<!}} \times \begin{cases} 1 + \dfrac{4x_0^2}{w^2}\left(\dfrac{4d^2}{w^2} - 1\right)\left(n + \dfrac{1}{2}\right) & \Delta n = 0 \\ \dfrac{4dx_0}{w^2} & |\Delta n| = 1, \\ \dfrac{2x_0^2}{w^2}\left(\dfrac{4d^2}{w^2} - 1\right) & |\Delta n| = 2 \end{cases} \tag{2}$$

where $n_<$ ($n_>$) is the lesser (greater) of $n$ and $n'$, and $x_0 \equiv \sqrt{\hbar/2m\omega}$ is the motional mode's ground state wavefunction size, with $m$ the mass and $\omega$ the secular frequency. We note that when $d = 0$ the Rabi frequency of all odd-order sidebands vanishes, as can be seen in equation (2) for $|\Delta n| = 1$. Exact expressions for $\Omega_{n',n}$ and are provided in appendix A.

In the Lamb–Dicke regime, a simple analytic expression describes the longitudinal spin–motion coupling, to lowest order in the Lamb–Dicke parameter $\eta \equiv k x_0$ (for wavevector $k$) [22]. We compare this to the case of transverse spin–motion coupling by defining an effective Lamb–Dicke parameter, $\tilde{\eta}_{(s)}$, where $s$ is the sideband order. As an example, if $d = w/2$, for the first order sidebands we have

$$\Omega_{n+1,n} = \tilde{\eta}_{(1)} \Omega_0 f(-w/2) \sqrt{n+1} \tag{3}$$

with

$$\tilde{\eta}_{(1)} \equiv \frac{2x_0}{w} \approx 0.014 \sqrt{\frac{100\ \mathrm{amu}}{m}} \sqrt{\frac{2\pi \times 1\ \mathrm{MHz}}{\Omega}} \frac{1\ \mu\mathrm{m}}{w}. \tag{4}$$

[1] Recent work has examined how a transverse electric field profile can drive an electronic, rather than motional, transition [20], and how spin angular momentum, rather than linear momentum, of photons can provide a momentum kick to trapped ions [21].

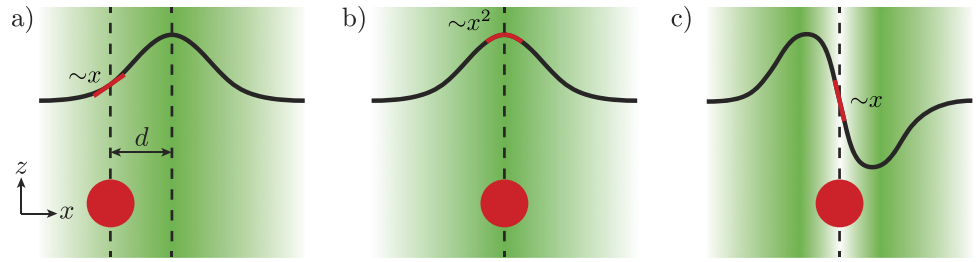


**Figure 1.** Schematic showing the geometry considered. A laser beam directed along $z$ is incident on a trapped ion (red). (a) and (b) Show the case where the interaction strength has a Gaussian ($TEM_{00}$) transverse profile (black solid line). Depending on the beam position, the profile at the ion can be approximately linear or quadratic (red solid line), coupling to first- or second-order sidebands, respectively. (c) Shows the case where the profile is produced by a $TEM_{10}$ mode, which suppresses carrier transitions while still coupling to motion.

When $d = 0$, the effective Lamb–Dicke parameter associated with the second-order sidebands has the same form ($\Omega_{n+2,n} \propto \tilde{\eta}_{(2)}^2/2$, with $\tilde{\eta}_{(2)} = 2x_0/w$). Unlike longitudinal spin–motion coupling from a plane wave, where the $p$th order sideband term is approximately proportional to $\eta^p/(p!)$, the expressions for the sideband strengths from transverse coupling are a function of the beam profile and position, and should be calculated individually for each sideband order.

The intuitive conclusion that we can draw is that transverse coupling to the ion motion is significant once the wavefunction size, $\sqrt{n}x_0$, becomes comparable to the transverse profile size, $w$. As the spatial extent of the beam becomes smaller, the corresponding transverse momentum spread of each photon increases, in accordance with the uncertainty principle, and the nonzero variance of this transverse momentum can change the transverse momentum of an ion without violating conservation of linear momentum. For the case of a stimulated Raman transition using a single focussed beam centred on the ion, one can associate an effective wavevector, $k_{\text{eff}} \equiv \tilde{\eta}/x_0 = 2/w_0$, with this momentum spread. An equivalent value of $k_{\text{eff}}$ can be achieved with two infinite plane waves crossing at an angle equal to the half-cone divergence angle of the single beam, $\theta \equiv \frac{\lambda}{\pi w_0}$, i.e. the coupling strength with the single focussed beam is half that for a pair of crossed plane waves defined by the same angular acceptance. This is a spatial manifestation of Ramsey's famous factor of two [23].

Having seen that transverse coupling to odd-order sidebands disappears with a centered $TEM_{00}$ beam, we now show that coupling to even-order sidebands (and carrier) can be extinguished if $f(x)$ is an odd function of $x$, such as with a $TEM_{10}$ mode (cf figure 1(c)) driving either a single photon transition (such as E2) or one of the arms of a stimulated Raman transition (with the other arm uniform intensity). Here, the Rabi frequency, $\Omega(x) \equiv \Omega_0 f(x)$, vanishes at the equilibrium position of the ion and has odd parity. For a $TEM_{10}$ beam with waist $w_0$, this configuration produces the same Rabi coupling for the single-photon and Raman cases, $f(x-d) \equiv H_1(\sqrt{2}(x-d)/w_0)\exp(-(x-d)^2/w_0^2) = 2\sqrt{2}\,\frac{x-d}{w_0}\,\exp(-(x-d)^2/w_0^2)$ where $H_1(x)$ is the first Hermite polynomial. Once again expanding to second order in $x_0$ gives the matrix elements for the carrier and the first and second sidebands:

$$\Omega_{n',n} = \Omega_0 2\sqrt{2}\,\mathrm{e}^{-d^2/w_0^2}\sqrt{\frac{n_>!}{n_<!}} \times \begin{cases} -\dfrac{d}{w_0}\left(1 - \dfrac{6x_0^2}{w_0^2}\left(1 - \dfrac{2d^2}{3w_0^2}\right)\left(n + \dfrac{1}{2}\right)\right) & \Delta n = 0 \\ \dfrac{x_0}{w_0}\left(1 - \dfrac{2d^2}{w_0^2}\right) & |\Delta n| = 1. \\ \dfrac{d}{w_0}\dfrac{3x_0^2}{w_0^2}\left(1 - \dfrac{2d^2}{3w_0^2}\right) & |\Delta n| = 2 \end{cases} \tag{5}$$

Since $f(x)$ is odd, when $d = 0$ the carrier and all even order sidebands vanish to all orders in $x_0$ (the exact expression for $\Omega_{n',n}$ and arbitrary order Hermite–Gaussian profile can be found in appendix A). This suggests that by switching between transverse spatial modes, the carrier or first sidebands can be suppressed as the application demands, which can be used to reduce undesired off-resonant effects. For example, using a $TEM_{10}$ could allow for Mølmer–Sørensen type gates [24] to be used at higher temperatures as the strengths of the carrier and second sidebands are greatly reduced. A related effect in the longitudinal direction has been explored for optical standing waves [22, 25–28], but the motional coupling in that case is still constrained to be along the longitudinal direction.

The appearance of sidebands (i.e. motional coupling) from the transverse spatial profile of a laser beam can be understood semi-classically in the time domain by considering that the oscillatory motion of an ion into and out of a laser beam gives an intensity modulation that produces sidebands at this oscillation frequency, which can in turn drive motional-state-changing transitions. Alternatively, one can consider the

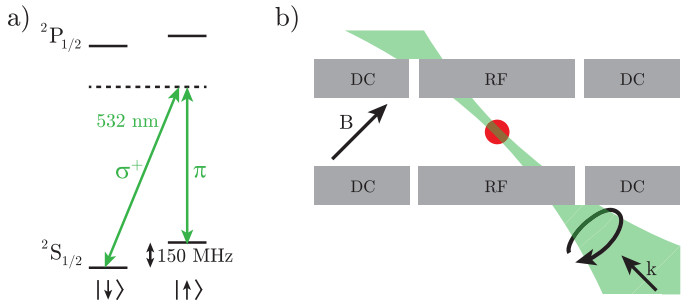


**Figure 2.** (a) Structure of the $^{138}Ba^+$ Zeeman qubit showing the laser field applied to drive stimulated Raman transitions (b) schematic of ion trap showing two of the four segmented rods and the single circularly polarised beam used to drive the Raman transitions.

associated Bloch sphere. In a frame rotating at the qubit splitting, the Bloch vector precesses azimuthally at a frequency equal to the detuning, $\Delta$. With negligible ion motion, no significant population transfer occurs (assuming $\Omega \ll \Delta$). With ion oscillation comparable to the beam size, the Rabi frequency will be modulated at $\omega$ and $2\omega$, associated with the linear and quadratic parts of $f(x)$, respectively. When $\Delta = \omega$, or $2\omega$, the precession and intensity modulation are synchronized. The result is a Bloch vector that 'spirals' up or down the Bloch sphere even for $\Omega \ll \Delta$ [see supplemental material (https://stacks.iop.org/QST/6/024003/mmedia)].

## 3. Experiment

The analysis we have presented indicates that if motional coupling can be driven by the transverse profile of a laser beam, sidebands should appear even for a co-propagating stimulated Raman transition (for our setup, this gives a longitudinal Lamb–Dicke parameter of $\eta \approx 10^{-7}$; note that the two frequencies required for the Raman transition are produced by the laser's pulsed nature, ensuring collinearity). The experiment we perform to observe these sidebands is shown schematically in figure 2. Briefly, we trap a single laser-cooled $^{138}Ba^+$ ion in a linear Paul trap made with four segmented cylindrical rods. The diagonal surface-to-surface distance between the rods is $2r_0 = 2$ cm. RF voltages are applied to the central segments at a frequency of 1 MHz to produce radial secular frequencies $\omega_{rad} \approx 2\pi \times 100$ kHz. The axial secular frequency is $\omega_{ax} = 2\pi \times 36$ kHz.

We define a Zeeman qubit with the two electron spin states ($|\downarrow\rangle$, $|\uparrow\rangle$) of the $^2S_{1/2}$ ground state manifold, which are split by 151.8 MHz by the application of a magnetic field of around 5.5 mT. Preparation of the qubit states is performed via optical pumping with circularly polarised light on the $^2S_{1/2} \leftrightarrow ^2P_{1/2}$ transition. Readout of the qubit state is achieved via electron shelving; circularly polarised light at 455 nm selectively optically pumps one of the qubit states to the long lived ($\tau \approx 30$ s) $^2D_{5/2}$ manifold via the $^2P_{3/2}$ manifold. Coherent transfer between the qubit states is driven by a far-detuned stimulated Raman transition via a mode-locked Nd:$YVO_4$ laser[2]. The qubit splitting is close to twice the repetition rate of the laser such that different frequency components of the laser light can resonantly drive the qubit transition when the magnetic field tunes the qubit splitting into resonance. Using the frequency comb structure of a mode-locked laser for this type of manipulation has previously been demonstrated in work with hyperfine qubits [29], but to our knowledge this is the first application to a Zeeman qubit[3].

To observe sidebands, we direct a single (i.e. 'co-propagating') circularly polarised beam at 45° to the axis of the trap and at 90° degrees to the quantization axis defined by the applied magnetic field (see figure 2). Even though none of the principal axes of the trap is perpendicular to the laser beam, traditional (i.e. longitudinal) spin–motion coupling will be effectively absent for this co-propagating geometry, and the appearance of sidebands will be entirely due to transverse spin–motion coupling. We perform Rabi spectroscopy on the Raman transition by measuring the spin flip probability while varying the applied magnetic field with a shim coil.

[2] Coherent Paladin SCAN 532-36000.

[3] A mode-locked laser has been used to coherently manipulate a Zeeman qubit, but employing acousto-optic elements to generate the necessary beat note [30].

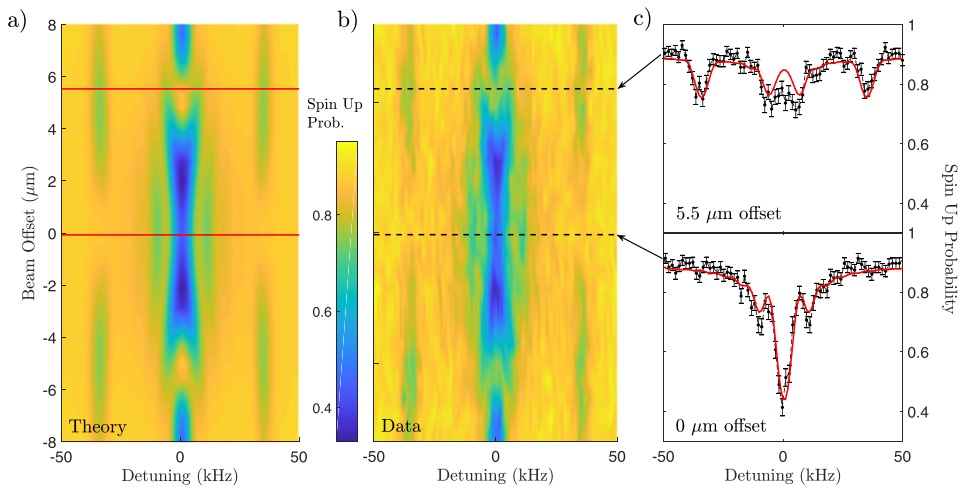


**Figure 3.** Appearance of transverse spin–motion coupling from a misaligned beam. (a) Calculated and (b) measured single-beam stimulated Raman spectra of the qubit as a function of beam position show sidebands for axial ion motion when the beam is off center. Horizontal lines indicate the slices shown in (c). The only free parameter used to generate the theory plots is the ion's motional temperature, which is 3 mK.

Figure 3 shows the probability of a stimulated Raman transition (with state preparation and measurement errors included) as a function of the detuning and beam offset. When the beam is misaligned, sidebands associated with motion along the trap axis are clearly visible at detunings of $\pm 36$ kHz, equal to the axial secular frequency. These sidebands vanish when the beam is centered on the ion as the gradient of the beam profile disappears, cf figure 1.

The plot in figure 3(a) shows the numerical solution of the Schrodinger equation with Rabi frequencies calculated as previously described. The ion temperature is the only free parameter used to match the experimental data (see supplemental material). The transverse Lamb–Dicke parameter for the first-order axial sideband ranges from $\tilde{\eta}_{(1)} = 0$ to 0.021 in figure 3. While this Lamb–Dicke parameter is small, the 3 mK mean occupation number of $\bar{n}_z = 1800$ can produce significant transverse motional coupling.

## 4. Discussion

Spin–motion coupling due to the transverse electric-field profile presents an additional tool with which to manipulate trapped ions. However, it may also represent an additional source of infidelity in trapped ion quantum computers. In many cases, single-site addressability is required and achieved via tightly focused laser beams which introduces spin–motion coupling for the transverse directions. It has already been shown that residual motion transverse to such beams can produce gate infidelities [31], but we now draw attention to the possibility that these beams can also impart momentum in the transverse directions. With reference to figure 4, we consider as an example the trapped ion quantum processor of Debnath *et al* [32]. Individual $^{171}Yb^{+}$ ions, spaced by $s \approx 5$ $\mu$m in a trap with axial secular frequency $\omega/2\pi = 270$ kHz, are addressed by a pair of stimulated Raman beams. One of the beams provides a uniform intensity, while the other has waist $w_0 \approx 1.5$ $\mu$m. Assuming a misalignment of $d = w/2$, we use equation (2) to calculate the transverse Lamb–Dicke parameters associated with the target ion to be $\tilde{\eta}_{(1)} \approx 0.0098$ and $\tilde{\eta}_{(2)} = 0$ for the first and second sidebands, respectively. Similarly for the neighbouring ion, $\tilde{\eta}_{(1)} \approx 0.037$ and $\tilde{\eta}_{(2)} \approx 0.035$. If the quoted crosstalk in [32] of 4% (interpreted as the ratio of carrier Rabi frequencies between adjacent ions) were solely due to beam misalignment, this would imply $d \approx 1.8$ $\mu$m and hence $\tilde{\eta}_{(1)} \approx 0.017$, $\tilde{\eta}_{(2)} \approx 0.014$ ($\tilde{\eta}_{(1)} \approx 0.030$, $\tilde{\eta}_{(2)} \approx 0.028$) for the target (neighbouring) ion. Transverse spin–motion coupling would, in general, lead to residual spin–motion entanglement in a two-qubit gate. We estimate that for a Mølmer–Sørensen type interaction [24, 33], with the parameters we have outlined and assuming the axial modes are cooled to the Doppler limit, this would produce an infidelity at approximately the $10^{-5}$ level. While this is too small to be of concern, it could become problematic for longer ion chains, or for traps where the axial modes are less far detuned from the mode used for computation; a fourfold reduction in detuning would produce an infidelity at the $10^{-3}$ level.

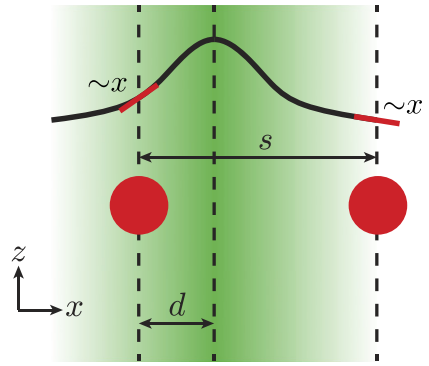


**Figure 4.** Laser incident on two ions, misaligned from a 'target' ion (left) by $d$. The transverse spatial profile of the interaction strength is approximately linear for both the target ion and the neighbouring ion, which can produce spin–motion coupling along the $x$ direction.

## Acknowledgments

This work was supported by the Office of Naval Research (award N000141712256) and the Defense Advanced Research Projects Agency (award D18AP00067).

## Appendix A. Exact expression for transverse Rabi frequency

While the use of a Taylor series in equations (2) and (5) provides intuition about how coupling between motional states depends on the transverse profile, an exact analytic expression for the Rabi frequency also exists. The equations below give the Rabi frequency associated with driving a transition from motional state $n$ to motional state $n'$ using transverse spin–motion coupling from a laser beam with a specific transverse spatial mode (along the motional mode direction) that is displaced by a distance $d$ from the trap centre. We write the Rabi frequency in terms of the function $J_{n',n,p}$ as

$$\frac{\Omega_{n',n,p}}{\Omega_0} = \langle n'|H_p\left[\sqrt{2}(x-d)/w_0\right] \mathrm{e}^{-(x-d)^2/w^2}|n\rangle = \frac{J_{n',n,p}(\alpha,\beta,\delta)}{\sqrt{\pi}\, 2^{n'+n}\, n'!\, n!} \tag{A.1}$$

where

$$\alpha(w) \equiv \left(\frac{2x_0}{w}\right)^2, \quad \beta \equiv \frac{2x_0}{w_0}, \quad \text{and} \quad \delta \equiv \frac{d}{\sqrt{2}x_0}. \tag{A.2}$$

(Recall that in the case of a Raman transition with one $\mathrm{TEM}_{p0}$ beam and one $\mathrm{TEM}_{00}$ beam, we identify $w = w_0$, whereas for either a Raman transition with one $\mathrm{TEM}_{p0}$ beam and one uniform beam, or for a single-photon transition driven by a $\mathrm{TEM}_{p0}$ beam, we use $w = \sqrt{2}w_0$.) The integral $J_{n',n,p}$ is given by

$$J_{n',n,p}(\alpha,\beta,\delta) \equiv \int_{-\infty}^{\infty} \mathrm{d}\xi\, \mathrm{e}^{-\alpha(\xi-\delta)^2-\xi^2} H_{n'}(\xi)\, H_n(\xi)\, H_p(\beta(\xi-\delta)) \tag{A.3}$$

$$\begin{aligned}
&= \sqrt{\frac{\pi}{1+\alpha}} \exp\left[\frac{\alpha^2\delta^2}{1+\alpha} - \alpha\delta^2\right] n'!n!\,p! \\
&\times \sum_{s=0}^{\min[n',n]} \sum_{q=0}^{\min[n'-s,p]} \sum_{r=0}^{\min[n-s,p-q]} \left\{ \frac{\left(\frac{2}{1+\alpha}\right)^{s+q+r} \beta^{q+r} (-i)^{n'+n+p-2(s+q+r)}}{s!\, q! r! (n'-s-q)! (n-s-r)! (p-q-r)!} \right. \\
&\times \left(\frac{-\alpha}{1+\alpha}\right)^{(n'+n-q-r-2s)/2} \left(\frac{\beta^2}{1+\alpha} - 1\right)^{(p-q-r)/2} \\
&\left. \times H_{n'-s-q}\left(\delta\sqrt{\frac{\alpha}{1+\alpha}}\right) H_{n-s-r}\left(\delta\sqrt{\frac{\alpha}{1+\alpha}}\right) H_{p-q-r}\left(\beta\delta \frac{\left(\frac{\alpha}{1+\alpha} - 1\right)}{\sqrt{1-\frac{\beta^2}{1+\alpha}}}\right) \right\},
\end{aligned} \tag{A.4}$$

where $\xi = x/\sqrt{2}x_0$ has been used as a normalised spatial coordinate.

To compare different values of $p$ for the same optical power in the $\mathrm{TEM}_{p0}$ mode, equation (A.1) should be multiplied by $1/\sqrt{p!\,2^p}$. In this case, the effective Lamb–Dicke factor for the first order sideband in the regime where $w_0 \gg x_0\sqrt{n}$ scales approximately as $\tilde{\eta}_{(1)} \propto p^{\frac{1}{4}}$.

## ORCID iDs

Adam D West https://orcid.org/0000-0003-4098-0165

## References


[1] Bruzewicz C D, Chiaverini J, McConnell R and Sage J M 2019 *Appl. Phys. Rev.* **6** 021314
[2] Leibfried D, Blatt R, Monroe C and Wineland D 2003 *Rev. Mod. Phys.* **75** 281–324
[3] Romaszko Z D, Hong S, Siegele M, Puddy R K, Lebrun-Gallagher F R, Weidt S and Hensinger W K 2020 *Nat. Rev. Phys.* **2** 285–99
[4] Seidelin S *et al* 2006 *Phys. Rev. Lett.* **96** 253003
[5] Wesenberg J H 2008 *Phys. Rev.* A **78** 063410
[6] Labaziewicz J, Ge Y, Antohi P, Leibrandt D, Brown K R and Chuang I L 2008 *Phys. Rev. Lett.* **100** 013001
[7] Allcock D T C *et al* 2010 *New J. Phys.* **12** 053026
[8] Stick D, Fortier K M, Haltli R, Highstrete C, Moehring D L, Tigges C and Blain M G 2010 Demonstration of a microfabricated surface electrode ion trap (arXiv:1008.0990)
[9] Pagano G *et al* 2019 Quantum approximate optimization of the long-range Ising model with a trapped-ion quantum simulator (arXiv:1906.02700)
[10] Gorman D J, Schindler P, Selvarajan S, Daniilidis N and Häffner H 2014 *Phys. Rev.* A **89** 062332
[11] Narayanan S, Daniilidis N, Möller S A, Clark R, Ziesel F, Singer K, Schmidt-Kaler F and Häffner H 2011 *J. Appl. Phys.* **110** 114909
[12] Ospelkaus C, Langer C E, Amini J M, Brown K R, Leibfried D and Wineland D J 2008 *Phys. Rev. Lett.* **101** 090502
[13] Ospelkaus C, Warring U, Colombe Y, Brown K R, Amini J M, Leibfried D and Wineland D J 2011 *Nature* **476** 181–4
[14] Harty T P, Sepiol M A, Allcock D T C, Ballance C J, Tarlton J E and Lucas D M 2016 *Phys. Rev. Lett.* **117** 140501
[15] Sutherland R T, Srinivas R, Burd S C, Leibfried D, Wilson A C, Wineland D J, Allcock D T C, Slichter D H and Libby S B 2019 *New J. Phys.* **21** 033033
[16] Zarantonello G, Hahn H, Morgner J, Schulte M, Bautista-Salvador A, Werner R F, Hammerer K and Ospelkaus C 2019 *Phys. Rev. Lett.* **123** 260503
[17] Srinivas R, Burd S C, Sutherland R T, Wilson A C, Wineland D J, Leibfried D, Allcock D T C and Slichter D H 2019 *Phys. Rev. Lett.* **122** 163201
[18] Sutherland R T *et al* 2020 *Phys. Rev.* A **101** 042334
[19] Ozeri R *et al* 2007 *Phys. Rev.* A **75** 042329
[20] Schmiegelow C T, Schulz J, Kaufmann H, Ruster T, Poschinger U G and Schmidt-Kaler F 2016 *Nat. Commun.* **7** 12998
[21] Afanasev A, Carlson C E and Mukherjee A 2020 Recoil momentum effects in quantum processes induced by twisted photons (arXiv:2007.05816)
[22] Wineland D J, Monroe C, Itano W M, Leibfried D, King B E and Meekhof D M 1998 *J. Res. Natl Inst. Stand. Technol.* **103** 259–328
[23] Kleppner D 2013 *Phys. Today* **66** 25–6
[24] Mølmer K and Sørensen A 1999 *Phys. Rev. Lett.* **82** 1835–8
[25] Cirac J I, Blatt R, Zoller P and Phillips W D 1992 *Phys. Rev.* A **46** 2668–81
[26] James D F V 1998 *Appl. Phys.* B **66** 181–90
[27] Reimann R, Alt W, Macha T, Meschede D, Thau N, Yoon S and Ratschbacher L 2014 *New J. Phys.* **16** 113042
[28] Uruñuela E, Alt W, Keiler E, Meschede D, Pandey D, Pfeifer H and Macha T 2020 *Phys. Rev.* A **101** 023415
[29] Hayes D *et al* 2010 *Phys. Rev. Lett.* **104** 140501
[30] Inlek I V, Crocker C, Lichtman M, Sosnova K and Monroe C 2017 *Phys. Rev. Lett.* **118** 250502
[31] Cetina M, Egan L N, Noel C A, Goldman M L, Risinger A R, Zhu D, Biswas D and Monroe C 2020 Quantum gates on individually-addressed atomic qubits subject to noisy transverse motion (arXiv:2007.06768)
[32] Debnath S, Linke N M, Figgatt C, Landsman K A, Wright K and Monroe C 2016 *Nature* **536** 63–6
[33] Sørensen A and Mølmer K 1999 *Phys. Rev. Lett.* **82** 1971–4